# Comparative study of three–dimensional localization accuracy in conventional, confocal laser scanning and axial tomographic fluorescence light microscopy

Joachim Bradl, Bernd Rinke, Arif Esa, Peter Edelmann, Hans Krieger,
Bernhard Schneider, Michael Hausmann, Christoph Cremer[+] *

Institute of Applied Physics,
University of Heidelberg, Albert–Ueberle–Str. 3–5,
D–69120 Heidelberg, Germany

[+] Interdisciplinary Centre for Scientific Computing (IWR),
University of Heidelberg, Im Neuenheimer Feld 368,
D–69120 Heidelberg, Germany

**key words:** conventional and confocal fluorescence light microscopy, spatial resolution, point spread function, axial tomography, quantitative image analysis

## ABSTRACT

For many biological applications, precise and accurate 3D object localizations and 3D–distance measurements are necessary. Point spread functions of artifical objects of subwavelength dimensions have been measured in order to characterize the image forming properties as well as to localize extended objects in both conventional and confocal fluorescence light microscopy with and without the axial tomographic technique. With the axial tomographic technique it is possible to tilt the object in such a way, that substructures are located in the same focal plane. The distance of two points measured under this optimal perspective fits best to the real 3D–distance. In this case, optical sectioning is unnecessary, if only distance measurements have to be performed.

## 1. INTRODUCTION

By means of fluorescence in situ hybridization (FISH, for reviews see: [1, 2]), it became possible to specifically label entire chromosomes, chromosomal subregions, individual genes, and sequences of ribonucleic acids in metaphase spreads and in cell nuclei. With this technique it has become possible to study the 3D organization of chromosomes in cell nuclei light microscopically. Exact three–dimensional (3D) localization measurements are basic requirements for these studies in quantitative fluorescence light microscopy. For conventional as well as for confocal laser scanning microscopy (CLSM), 3D–images are usually acquired by optical sectioning. The 3D–distance of objects can then be determined after segmentation. However, the theoretical mean error obtained with this procedure strongly depends on the accuracy of localization and on the object orientation itself [3].
The spatial resolution of a conventional light microscope or a CLSM can be determined either by calculating the "full width half maximum (FWHM)" of the "point spread function (PSF)" under the assumption of ideal optical conditions [4], or by measuring the PSF, e.g. with fluorescent microspheres of sub–wavelength dimensions [5, 6]. From these measurements, values for the lateral and axial FWHM of these point like objects are obtained. These FWHM values are an estimate of the experimentally realized spatial resolution. Due to physical reasons the axial

*Correspondence to Prof. Dr. C. Cremer, Institute für Angewandte Physik, Albert–Ueberle–Str. 3–5, D–69120 Heidelberg, Germany

0-8194-2328-9/96/$6.00

resolution is reduced compared to the lateral resolution in theoretically as well as in experimentally determined PSFs of the epifluorescence and the confocal microscopes.
To overcome this problem, axial tomography can be applied [3, 6, 7]. With this technique it is possible to physically tilt biological specimens around one lateral axis with a $2\pi$–geometry (0–360°) using microscope lenses of high numerical aperture. The objects are located either inside a quartz glass capillary or fixed on a glass fibre. The tilting device carrying the capillary/fibre can be mounted onto a variety of microscope stages, available for conventional as well as for confocal microscopes. Since the object can be tilted into an optimal perspective, this technique enables a discrimination of substructures which are located close to each other, especially in cases where their distance is $\leq$ 1 axial FWHM but $\geq$ 1 lateral FWHM.
This is especially helpful for clinical applications. For instance, in hematology tumor cells are often correlated with chromosome aberrations, e.g. chronic and acute myelogenous leukaemia with trisomy 8 [8] or B–cell chronic lymphocytic leukaemia with trisomy 12 [9, 10]. Another prominent example is the philadelphia chromosome (9/22 translocation) with the abl–bcr breakpoint regions [11]. With FISH it has become possible to specifically label the chromosome aberrations directly in cell nuclei with high sensitivity. However, the demands for high resolution and precision microscopy are high. "Optical fusion" of fluorescently labelled targets of unknown size and shape closely located together has to be clearly discriminated from the real association of the targets. This demand can often not be fulfilled from an image acquired in one perspective only. Also highly sophisticated computer image analysis cannot fully overcome acquisition shortcomings. Thus, image registration under several or under one optimal perspective should be applied. Comparative results for artificial objects of well known shape are described elsewhere [12].
In this study we investigated experimentally the accuracy of localization due to the image segmentation process being applied. This segmentation accuracy gives a lower limit for the error of distance determination which may depend on the microscope setup used.

## 2. MATERIAL AND METHODS

An *experimental* estimate for the accuracy of localization can be found in two ways: one way is to measure a number of objects for each setup with exactly the same distances and to determine the error statistically. The other way is to measure some individual objects for each setup and to evaluate the error in the localization of those objects, depending on the segmentation threshold. In the following the latter procedure will be applied.

### 2.1. Object preparation

Quantitative distance measurements of `(i)` calibration objects (latex beads) and `(ii)` biological objects (fluorescently labelled targets in cell nuclei) were carried out using `(a)` an epifluorescence microscope (conventional) and `(b)` a confocal laser scanning microscope (CLSM) with and without the axial tomographic technique. This lead to eight different cases as given in the following table:

| Object Slide | | | | Axial tomograph | | | |
|---|---|---|---|---|---|---|---|
| Conventional | | CLSM | | Conventional | | CLSM | |
| Beads | Nuclei | Beads | Nuclei | Beads | Nuclei | Beads | Nuclei |

Fluorescent latex spheres (Polyscience Inc., USA) with a diameter of 1 $\mu$m, labelled with a fluorochrome suitable for FITC (Fluoresceinisothiocyanat) excitation and detection were used as calibration objects `(i)`. They were dropped on cover slides and after air drying the cover slide was mounted upside down onto an object slide with glycerol as a mounting medium. For fixation on borosilicate glass fibres, the fibre was dived into a water solution containing beads; an adequate bead concentration resulted in only a few isolated beads on the fibre surface in the image field. The fibre was mounted into the tilting device and a glycerol–water immersion fluid was used in order to match the refractive index of the fibre. After adding a cover slide, the tilting device was mounted onto the microscope stage. Immersion oil was put between the cover slide and the objective lens.
For biological objects `(ii)`, interphase nuclei of peripheral blood lymphocytes and bone marrow cells from patients with hematological disorders were used. In order to detect numerical aberrations of chromosome 8 and 12, the centromere regions of those chromosomes were labelled specifically with commercially available $\alpha$–satellite DNA probes. The recently developed Fast FISH procedure [13, 14] was applied. In order to prepare the cell nuclei on the glass fibre, the fibre was placed on an object slide. This was sufficient for attachment of the nuclei on the fibre as well as for the Fast FISH procedure. Labelling of the major binding sites resulted in two or three fluorescence

spots (FITC) within a cell nucleus. The cell nuclei were counterstained with PI (propidium iodide), which could be detected with a lower intensity using the same chromatic filter set in the conventional epifluorescence microscope.

### 2.2. Imaging equipment

The epifluorescence microscope (a) was a Zeiss Standard 25 with a HBO 50 W mercury lamp. It was equipped with filter sets for FITC and TRITC (Tetramethylrhodaminisothiocyanat) fluorescence illumination and detection; a Zeiss 100×/1.32 objective lens for oil immersion was used. The tilting device had been adapted to a step motor controlled xy–stage (Fa. Märzhäuser, Wetzlar, FRG). For optical sectioning, the stage was moved in axial direction by a step motor directly coupled to the standard microscope focusing mechanics. The xy–movement of the stage and the z–focus were controlled by a transputer unit (MC 2000, Fa. ITK, Lahnau, FRG) and operated either by a joystick or by computer program. Each step motor had a resolution of 40 000 steps for 360°. An area of 75×25 mm (xy–plane) could be scanned with a minimum theoretical step width of 0.01 $\mu$m and a reproducibility for relocation of $\pm$0.5 $\mu$m. The minimum step size of the focusing unit (z–axis) was measured by means of a differential–incremental unit (Fa. Messotron, Seeheim, FRG) to 200 nm with a reproducibility of $\pm$60 nm over an axial distance of 13 mm. For image acquisition, a cooled black and white CCD camera (CF 8 RC; Fa. Kappa, Gleichen, FRG) was used. The interline transfer CCD chip had a size of 8.8×6.6 mm, 739×575 pixels (x–y) and a pixel size of about 11×11 $\mu$m. The CCD camera was read out via a MFG–3M–AVS frame grabber board in single monitor display mode (Imaging Technologies Inc., MA, USA).

The complete setup was operated by a 50 MHz 80486 personal computer equipped with 8 MByte RAM and a 870 MByte IDE hard disk. For automated image acquisition, an acquisition program was developed under MS–DOS using the ITEX Library (Imaging Technologies Inc., MA, USA), which synchronized image recording and storage with the step motor controlled focusing.

The Leica CLSM TCS 4D (b) was equipped with an air cooled Ar–Kr ion laser, which was used for excitation of the fluorochrome FITC at a wavelength of 488 nm. The fluorescence emission was detected with a filter set appropriate for the FITC fluorochrome. The cell nuclei which were counterstained with PI fluorochrome were excited at a wavelength of 568 nm. A Leitz objective lens PL APO 100×/0.7–1.4 for oil immersion with an NA setting corresponding to 1.4 was used.

The image forming properties (PSFs) of both microscopes were experimentally determined with and without the axial tomographic setup ([3, 15]).

### 2.3. Image acquisition

The following parameters for image acquisition were commonly set to all measurements for each microscope: objective lens being used; focal step width for optical sectioning; electronic zoom (CLSM) resulting in the same pixel size; integration or averaging time. The dynamic range of all images was 8 Bit.

For the epifluorescence microscope (a), the following parameters were used: xy–pixel size of 109 nm; z–step width of 300 nm; integration time for beads was 1 full frame image (40 ms); for cell nuclei 2 to 5 images were integrated (depending on signal to noise ratio). The average time for image acquisition of a data stack of 100 images was about 3 minutes, mainly limited by the storage duration of the image data onto the hard disc. The region of interest was set individually for each object, mostly to about 200×200 pixels.

The parameters for the CLSM (b) were set to: xy–pixel size of 100 nm; z–step width of 200 nm; a line average of eight times was chosen; the laser power and the pinhole diameter were kept constant; gain and offset of the amplifier of the photomultiplier were adjusted depending on signal to noise ratio of the object. The average acquisition time for a data stack of about 40 images was about 4 minutes, each image plane had a size of 256×256 pixels.

Up to 38 different images were acquired. More than two beads or labelled targets were acquired per image, resulting in more than 80 localization measurements.

### 2.3. Image analysis

For each global threshold within a selected range of possible thresholds, the image was analyzed by means of object identification and the centre of mass coordinates of the resulting objects were extracted. The selection of the threshold range was performed interactively, in order to control the segmentation result.

Depending on the threshold, the centre of mass coordinates $(x_i, y_i, z_i)$ varied; the standard deviation (SD) of this variation $\delta x_i, \delta y_i, \delta z_i$ was interpreted as the variation of object localization. The average error of the 3D–distance measurement $\delta D_{xyz}$ for each case was estimated as the arithmetic average of the SD of the centre of mass coordinates $\delta x_i, \delta y_i, \delta z_i$.

## 3. RESULTS

The localizations of all objects were analyzed in the 3D images by means of threshold segmentation. The localization error of the objects expressed by the SD of the centre of mass coordinates varied considerably. Preliminary results of the means of all values are given in Table 1 and Table 2.

For the axial tomographic setups, two kinds of values are given: The mean value of all images and the mean value of a "zero position" perspective. In contrast to the object slide setup, the axial tomography allowed rotation to a perspective where the objects of investigation were located in the best focal plane, for instance in a configuration with a minimal value of the z–coordinate distance (= "zero position"). This basic advantage of axial tomography justified the unusual comparison of the average mean values (slide setup) to optimal "zero position" values (axial tomographic setup).

For the beads measurements (Table 1), $\delta xy$ was about the same for the object slide and the axial tomographic setup. $\delta z$ was considerably better for the CLSM than for the epifluorescence microscope. However, due to the reduction of the $\delta z$ by axial tomography, $\delta D_{xyz}$ was at least about half the value of standard epifluorescence setup with slide.

| | Conventional | | | CLSM | | |
|---|---|---|---|---|---|---|
| | Object Slide | Axial tomography | | Object Slide | Axial tomography | |
| $\delta xy$ | 6.5 | 7.8 | 6.7 | 7.4 | 12.1 | 7.6 |
| $\delta z$ | 36.2 | 58.5 | 34.0 | 19.2 | 21.7 | 11.4 |
| $\delta D_{xyz}$ | 16.4 | 24.7 | 15.8 | 11.4 | 15.3 | 8.9 |

Table 1: Error in localization measurement for fluorescent beads

Comparison of the average errors obtained by the localization measurement of beads. $\delta xy$ gives the SD of the localization in the focal plane; $\delta z$ the SD in direction of the optical axis; $\delta D_{xyz}$ is the SD of the 3D–distance; the left column for the axial tomography indicates the average for all cases, the right column shows an optimal value for a typical "zero position" (for details see text). All values are given in nm.

| | Conventional | | | CLSM | | |
|---|---|---|---|---|---|---|
| | Object Slide | Axial tomography | | Object Slide | Axial tomography | |
| $\delta xy$ | 20.2 | 23.8 | 10.8 | 33.8 | 25.4 | 7.8 |
| $\delta z$ | 92.8 | 181.4 | 62.2 | 39.2 | 39.2 | 20.4 |
| $\delta D_{xyz}$ | 44.4 | 76.3 | 27.9 | 35.6 | 30.0 | 12.0 |

Table 2: Error in localization measurement for biological objects

Comparison of the average errors obtained by the localization measurement of cell nuclei with fluorescence labelled targets. $\delta xy$ gives the SD of the localization in the focal plane; $\delta z$ the SD in direction of the optical axis; $\delta D_{xyz}$ is the SD of the 3D–distance; the left column for the axial tomography indicates the average for all cases, the right column shows an optimal value for a typical "zero position" (for details see text). All values are given in nm.

The improvement in microscopy by axial tomography became transparent analyzing FISH labelled targets in cell nuclei (ii). The five images of Fig. 1 show extended views of one cell nucleus with two labelled targets at five different angles of rotation ($-90°, -45°, 0°, +45°, +90°$). In the $-45°$ and $0°$ image, the two labelling sites were not clearly distinguishable. For geometrical reasons, the true distance (3D–distance) is the largest one ($+45°$ position). There, the two targets are in the same focal plane which corresponds to the "zero position". As Table 2 indicates, the accuracy of localization was improved considerably. Also $\delta xy$ was reduced by about a factor of 2. This indicated that the focal shift due to refraction index mismatch by the nucleus chromatin had an influence of the localization accuracy depending on the position of the labelling site (i.e. in an upper or lower focal plane). This was overcome by rotation to a "zero position" (i.e. best upper plane). For the conventional axial tomographic setup, $\delta D_{xyz}$ values were obtained in the range of the values measured by the CLSM.

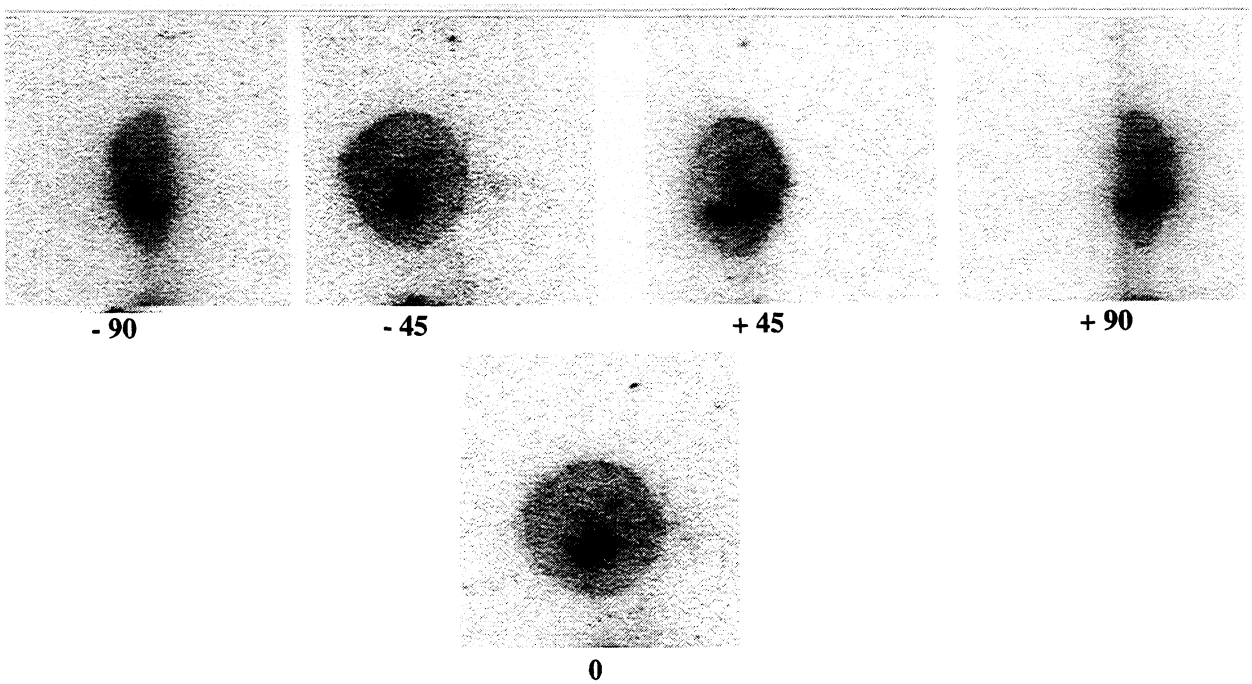


Figure 1: The same cell nucleus on a glass fibre under five different perspectives

Five different perspectives (above, from left to right: $-90, -45°, +45°, +90°$, below: $0°$) of the same cell nucleus attached to a glass fibre with 2 labelled regions after 3D confocal image acquisition, segmentation and visualization. It is not possible to distinguish the two target regions in the $-45°, 0°$ position, whereas this is obvious in the other perspectives. The images are given in false colours (inverse look–up–table).

## 4. DISCUSSION

For many biological applications, precise 3D–location and 3D–distance measurements of various structures and objects are necessary. A lower limit of the 3D–distance error is given by the accuracy of localization of the objects. This accuracy was determined in both conventional and confocal fluorescence light microscopy. Beads as well as cell nuclei with specifically labelled fluorescent targets were used. Application of the axial tomographic technique resulted in an additional method to compare values for the different setups. The overall results show that there is a considerable high variability in the average errors found.

For beads (spherical objects with high fluorescence intensity), the corresponding localization errors were similar for the different setups. The smallest errors were obtained for the xy–directions. In the conventional setups, the 3D–arrangement of the objects cannot be influenced. Hence, the error in 3D–distance measurements depends on the error in the 3D–localization. In axial tomography, however, the objects can be rotated to the "zero position". The error of the 3D–distance measurement depends almost exclusively on the xy–localization error only (best case in the order of a few nm only). These results are compatible with results obtained by [16].

The results obtained for fluorescence labelled targets *within* cell nuclei essentially confirm the results obtained with beads. However, the error margins obtained here were considerably larger. Moreover,the results show that in cases of localization analysis where real 3D–image visualization might not be required, the advantages of the CLSM may be marginal compared to optimal practical conditions in a high quality epifluorescence microscope with axial tomography. However, this has to be proven by more images with different types of labelling sites.

It should be mentioned that the data sets presented here are based on a relatively low number of images considering the laws of statistics. Thus, the data have to be seen as preliminary. However, they clearly show the tendencies and confirm the basic advantages of axial tomography application proposed by [3, 6, 7]. To give an absolute estimate for localization and resolution limits especially in biological specimen a higher amount of data have to be processed. This will be the goal for future studies.

## 5. ACKNOWLEDGEMENTS

The financial support of this study by the Deutsche Forschungsgemeinschaft is gratefully acknowledged. B. Rinke receives a DFG scholarship as a member of a DFG graduate college.
We thank Prof. T. Cremer, Institute of Anthropology and Human Genetics, University Munich, for the access to the confocal laser scanning microscope TCS 4D and Dr. L. Trakhtenbrot, Institute of Hematology, Tel Hashomer (University Tel Aviv) for the bone marrow cell preparations.

## References

[1] P. Lichter, A.L. Boyle, T. Cremer, and D.C. Ward. Analysis of genes and chromosomes by non–isotopic in situ hybridization. *Genet. Anal. Techn. Appl.*, 8:24–34, 1991.

[2] C. Cremer and T. Cremer. Analysis of chromosomes in molecular tumor and radiation cytogenetics: Approaches, applications, perspectives. *Europ. J. Histochem.*, 36:15–25, 1992.

[3] J. Bradl, B. Rinke, M. Hausmann, B. Schneider, and C. Cremer. Improved resolution in "practical" light microscopy by means of a glass fibre $2\pi$–tilting device. *Proc. SPIE 2628*, 140–146, 1996.

[4] B. Richards and E. Wolf. Electromagnetic diffraction in optical systems II. Structure of the image field in an aplanatic system. *Proc. Roy. Soc.*, A 253:358–379, 1959.

[5] Y. Hiraoka, J.W. Sedat, and D.A. Agard. Determination of three-dimensional imaging properties of a light microscope system. Partial confocal behavior in epifluorescence microscopy. *Biophys. J.*, 57:325–333, 1990.

[6] J. Bradl, M. Hausmann, B. Schneider, B. Rinke, and C. Cremer. A versatile $2\pi$–tilting device for fluorescence microscopes. *J. Microsc.*, 176:211–221, 1994.

[7] J. Bradl, M. Hausmann, V. Ehemann, D. Komitowski, and C. Cremer. A tilting device for 3–D microscopy: application to in situ imaging of interphase cell nuclei. *J. Microsc.*, 168:47–57, 1992.

[8] A.M. Potter and A. Watmore. *Cytogenetics in myeloid leukaemia.* IRL Press at Oxford University Press, 1992.

[9] Ch. Geisler, P. Philip, and M.M. Hansen. B–CLL chronic lymphocytic leukaemia: Clonal chromosome abnormalities and prognosis in 89 cases. *Eur. J. Haematol*, 43:397, 1989.

[10] G. Juliusson and G. Gahrton. Chromosome aberrations in B–cell chronic lymphocytic leukaemia. Patologenetic and clinical implications. *Cancer. Genet. Cytogenet.*, 45:143–160, 1990.

[11] D. C. Tkachuk, C. A. Westbrook, M. Andreeff, T. A. Donlon, M. L. Cleary, K. Suryanarayan, M. Homge, A. Render, J. Gray, and D. Pinkel. Detection of bcr–abl fusion in chronic myelogeneous leukaemia by in situ hybridization. *Science*, 250:559–562, 1990.

[12] B. Rinke, J. Bradl, P. Edelmann, B. Schneider, M. Hausmann, and C. Cremer. Image acquisition and calibration methods in quantitative confocal laser scanning microscopy. *submitted to: Proc. SPIE, BIOS Europe 1996 Optoelectronic Research and Techniques: Optical Microscopic Techniques*, 2926–15.

[13] M. Durm, F.M. Haar, M. Hausmann, H. Ludwig, and C. Cremer. Optimization of fast–fluorescence in situ hybridization with repetitive alpha–satellite probes. *Z. Naturforsch.*, 51c:253–261, 1996.

[14] A. Esa, L. Trakhtenbrot, M. Hausmann, I. Ben-Bassat, and C. Cremer. Detection of trisomy 8, trisomy 12 and tetrasomy 8 in hematological disorders by fast fluorescence in situ hybridization (Fast–FISH) in interphase nuclei. *to be submitted.*

[15] B. Rinke, J. Bradl, B. Schneider, M. Durm, M. Hausmann, H. Ludwig, and C. Cremer. *Fluorescence Microscopy & Fluorescent Probes*, "In situ" estimates of the spatial resolution for "practical" fluorescence microscopy of cell nuclei, 178–183. Plenum Press, 1996.

[16] U. Kubitscheck, P. Wedekind, O. Zeidler, M. Grote, and R. Peters. Single nuclear pores visualized by confocal microscopy and image processing. *Biophys. J.*, 70:2067–2077, 1996.